Article:
Lübben, O, Krasnikov, SA, Walls, B et al. (5 more authors) (2017) Nanoclusters and nanolines: the effect of molybdenum oxide substrate stoichiometry on iron self-assembly. Nanotechnology, 28 (20). 205602. ISSN 0957-4484

https://doi.org/10.1088/1361-6528/aa6b50

Nanoclusters and Nanolines: the Effect of Molybdenum Oxide Substrate Stoichiometry on Iron Self-assembly

O Lübben[1], S A Krasnikov[1], B Walls[1,*], N N Sergeeva[2], B E Murphy[1], A N Chaika[1,3], S I Bozhko[1,3] and I V Shvets[1]

[1] School of Physics and Centre for Research on Adaptive Nanostructures and Nanodevices (CRANN), Trinity College Dublin, Dublin 2, Ireland
[2] School of Chemistry, University of Leeds, Leeds LS2 9JT, U.K.
[3] Institute of Solid State Physics, Russian Academy of Sciences, Chernogolovka, Russian Federation

E-mail: wallsb@tcd.ie

Abstract. The growth of Fe nanostructures on the stoichiometric MoO_2/Mo(110) and oxygen-rich MoO_{2+x}/Mo(110) surfaces has been studied using low-temperature scanning tunneling microscopy (STM) and density functional theory calculations. STM results indicate that at low coverage Fe nucleates on the MoO_2/Mo(110) surface, forming small, well-ordered nanoclusters of uniform size, each consisting of 5 Fe atoms. These 5-atom clusters can agglomerate into larger nanostructures reflecting the substrate geometry but retain their individual character within the structure. Linear Fe nanocluster arrays are formed on the MoO_2/Mo(110) surface at room temperature when the surface coverage is greater than 0.6 monolayers. These nanocluster arrays follow the direction of the oxide rows of the strained MoO_2/Mo(110) surface. Slightly altering the preparation procedure of MoO_2/Mo(110) leads to the presence of oxygen adatoms on this surface. Fe deposition onto the oxygen-rich MoO_{2+x}/Mo(110) surface results in elongated nanostructures that reach up to 24 nm in length. These nanolines have a zigzag shape and are likely composed of partially oxidized Fe formed upon reaction with the oxygen-rich surface.

PACS numbers: 68.37.Ef, 68.47.Gh, 62.23.St, 64.75.Yz

Keywords: molybdenum oxide, iron nanoclusters, self-assembly, scanning tunneling microscopy, density functional theory

1. Introduction

An understanding of the mechanisms of the controlled growth of surface-supported nanostructures is fundamental to progress in the fields of surface science and solid state physics. Such nanostructures could be vital to the design of novel devices and new technologies in the near future [1, 2, 3, 4]. They are also useful for the studies of catalysis on the nanoscale [5, 6]. Conventional catalytic systems make use of complex and heterogeneous materials. At the same time, less complex systems such as functional nanoparticles and nanoclusters grown in a highly controlled way on single-crystalline substrates, are of scientific interest as the effect of particle size and shape on catalytic activity can be tested in a systematic manner [7].

With the advent of highly localised techniques, such as scanning tunneling microscopy (STM) and density functional theory (DFT), catalysis can be studied on the nanoscale. For example, STM and DFT have recently been combined to describe the surface-supported Co-Mo-S model nanoparticle system, which is important for the industrially-significant hydrodesulfurization process, and it was shown that the size and shape of the nanoparticles very strongly affect their reactivity properties [8]. Indeed, nanoparticle size and shape has been demonstrated to hugely influence the catalytic behaviour and capability of substrate-nanoparticle systems [1, 7, 9, 10]. Furthermore, STM has also made it possible to observe adsorption of gas-phase molecules onto nanoclusters-substrate systems in real time and to explore the effect of edge states, nanoparticle size and defects on catalytic activity [11, 12, 13, 14]. Finally, the effects of edges [15], kinks [16], atomic vacancies [17, 18] and other defects have been probed and are now known to play a large role in catalytic performance. It is therefore paramount to understand the growth behavior of such nanoparticles and to be able to control the size, morphology and distribution of these active sites in order to test and optimise the catalytic capability.

Iron-based catalysts are used in many catalytic systems such as the splitting of the N_2 triple bond utilized in the Haber process [19] and the partial oxidation of methanol for the production of formaldehyde [20]. The efficiency of such mixed-phase reactions depends on the surface area of the catalyst available for the adsorption of reagents, thus nanoclusters of functional materials evenly distributed over a surface represent some of the highest surface area-to-volume ratios possible.

Oxide formation on transition metal (TM) surfaces has received considerable attention in recent years [21, 22, 23, 24]. TM oxide surfaces such as the $MoO_2(010)$ surface can be suitable templates for the growth of well-ordered, uniformly-sized metal nanoclusters [25]. The size, shape, and the spacing between clusters can be dictated by the substrate and growth conditions, and in turn size and shape effects can dictate the electronic structure of the clusters.

In the present work we use the stoichiometric $MoO_2(010)$ and oxygen-rich $MoO_{2+x}(010)$ surfaces as templates for the growth of ordered arrays of Fe nanostructures. We employ STM and DFT calculations to study the nucleation, structure and alignment of the Fe nanostructures. It is found that the oxygen content of the molybdenum oxide surface dictates the size and shape of the Fe nanostructures; Fe deposited on the $MoO_2(010)$ and $MoO_{2+x}(010)$ surfaces gives rise to the formation of nanoclusters and zigzag nanolines, respectively.

2. Experimental

The STM experiments were performed at liquid nitrogen temperature 78 K, using a commercial instrument from Createc, in an ultra-high-vacuum (UHV) system consisting of preparation and analysis chambers with base pressures of 5×10^{-10} mbar and 5×10^{-11} mbar, respectively. An electrochemically-etched monocrystalline W(100) tip [26, 27] was used to record STM images in constant current mode. The voltage, V_b, corresponds to the sample bias with respect to the tip. No drift corrections have been applied to any of the STM images presented in this paper.

A Mo(110) single crystal (Surface Preparation Laboratory) was used as the substrate. The lattice directions stated throughout the manuscript correspond to the surface vectors of this crystal. An atomically-clean Mo(110) surface was prepared by *in situ* annealing at 1500 K in an oxygen atmosphere of 1×10^{-6} mbar, followed by a series of high temperature flashes at 2200 K. The sample was heated by electron beam bombardment and temperatures were measured using an optical pyrometer (Ircon UX20P, emissivity 0.35). The clean Mo(110) surface was verified by

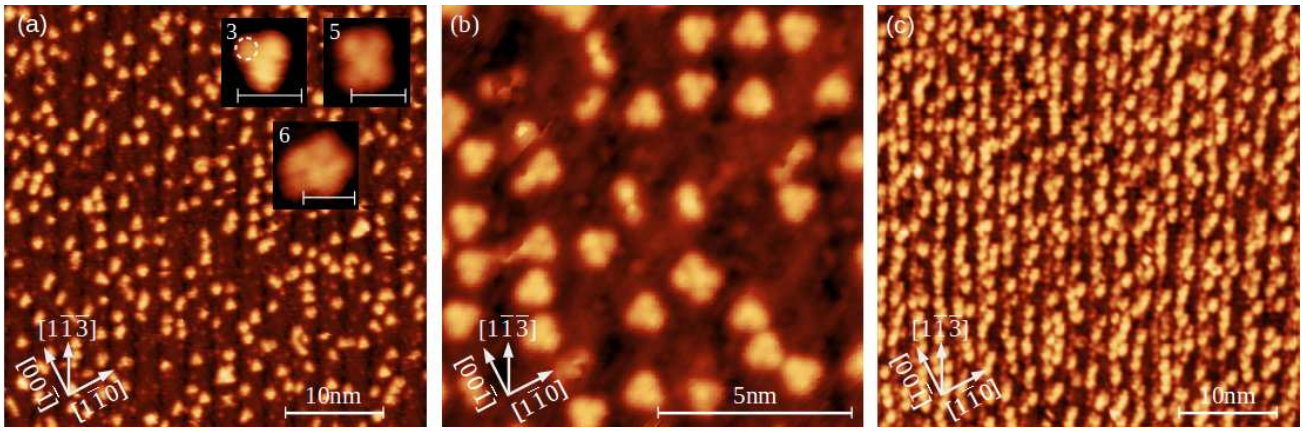

Figure 1. (a) STM image of 0.3 ML of Fe on MoO_2/Mo(110) (40 nm × 40 nm, V_b = - 0.5 V, I_t = 1.10 nA). Deposition of 0.3 ML of Fe on the MoO_2/Mo(110) surface leads to the formation of small nanoclusters, which appear round in shape and are 6 Å in width. Most of these Fe nanoclusters form larger entities comprised of multiples of small ones. Inserts show multiples of 3, 5 and 6 of the small Fe nanoclusters, the white dashed circle highlights one of the individual Fe nanoclusters. The scale bar in each of the 3 insets corresponds to 1.25 nm. All these nanostructures are located on top of the oxide rows, with a variable separation between them. (b) STM image of 0.3 ML of Fe on MoO_2/Mo(110) (10 nm × 10 nm, V_b = - 0.5 V, I_t = 1.10 nA). There is a clear preference for nanoclusters to agglomerate into triangular composite structures containing three individual nanoclusters. (c) STM images of 0.7 ML of Fe on MoO_2/Mo(110) (40 nm × 40 nm, V_b = 1.2 V, I_t = 1.00 nA). In this case the separation between nanoclusters on the MoO_2/Mo(110) surface becomes much smaller. At such coverage the Fe nanoclusters self-assemble into linear nanocluster arrays. These arrays follow the [1$\bar{1}$3] direction of the substrate oxide rows.

low energy electron diffraction (LEED) and STM before oxidation. Once a clean surface was obtained, the sample was oxidised at 1275 K in an oxygen atmosphere of 1×10^{-7} mbar for 2 minutes and allowed to cool in UHV. The quality of the resulting oxide structure was verified by LEED and STM. In order to obtain oxygen adatoms on the MoO_2/Mo(110) surface, the clean Mo(110) was oxidised at slightly lower temperature 1225 K in an oxygen atmosphere of 1×10^{-7} mbar for 2 minutes and cooled down in an oxygen atmosphere. Fe was deposited on the MoO_2/Mo(110) and MoO_{2+x}/Mo(110) surfaces from an electron-beam evaporator at a rate of 0.1 monolayer (ML) per minute. The substrates were kept at room temperature during deposition. After deposition, the sample was transferred into the STM and cooled down to 78 K.

3. Results and Discussion

3.1. Growth of Fe on the MoO_2/Mo(110) surface

MoO_2(010) grows epitaxially on the Mo(110) surface in the form of an O-Mo-O trilayer, which exhibits well-ordered oxide nanorows separated by 2.5 nm [28, 29]. These rows are oriented along the [1$\bar{1}$3] crystallographic direction of the Mo(110) surface. In STM images they appear as bright regions with dark depressions in between. Deposition of 0.3 ML of Fe on the MoO_2/Mo(110) surface leads to the formation of small nanoclusters (figure 1a). Individual nanoclusters appear round in shape and are 6 Å in width. They are located on top of the oxide rows, with a variable separation between them along the row direction. Most of these nanoclusters form larger composite structures comprised of several small Fe nanoclusters. Multiples of two, three, four, five, and six of the small Fe nanoclusters have been observed and examples are presented in figure 1(a) as inserts. It is noted that at low surface coverage there is a clear preference for the formation of triangular composite structures which contain 3 Fe nanoclusters. This

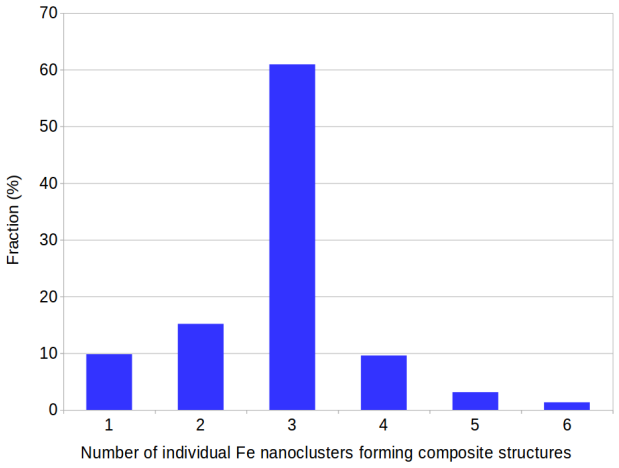

Figure 2. Statistical distribution of the probability of observing larger composite structures on the surface that consist of 1 to 6 individual Fe nanoclusters. Some 900 of these composite structures at the surface coverage of 0.3 ML were used for this statistical analysis. Examples of such composites containing 3, 5 and 6 Fe nanoclusters are shown in figure 1(a) as inserts.

can be clearly seen from figure 1(b), where the vast majority of nanostructures are comprised of three individual nanoclusters. Several STM images similar to that presented in figure 1(a) have been analysed and the number of nanoclusters within some 900 composite structures has been determined. Figure 2 illustrates the occurrence of 1, 2, 3, 4, 5 and 6 individual Fe nanoclusters within the composite structures for the surface coverage of 0.3 ML. The high probability of the formation of triangular composite structures originates from the structure of the MoO_2/Mo(110) substrate. The structure of the oxygen top layer greatly influences the spatial distribution of the Fe nanoclusters. This will be discussed later in detail with the help of the DFT-calculated models. In the case of higher Fe coverage (0.6 – 0.9 ML) the separation between composite nanostructures on the MoO_2/Mo(110) surface becomes much smaller. It is clear from figure 1(c) that at such coverage the Fe nanoclusters self-assemble into linear nanocluster arrays. These arrays follow the $[1\bar{1}\bar{3}]$ direction of the Mo(110) surface which coincides with the direction of the substrate oxide rows. It is noted that despite very small separation between the Fe nanoclusters (or multiple nanocluster composites) they do not form continuous Fe nanolines at such surface coverage (0.6 – 0.9 ML). This is due to low mobility of Fe atoms on the MoO_2/Mo(110) surface caused by interaction of the former with the oxygen top layer of the substrate.

DFT calculations were performed to identify the number of Fe atoms in the round-shaped nanoclusters formed on the MoO_2/Mo(110) surface. The Vienna *Ab initio* Simulation Package (VASP) software was used for these simulations. VASP implements a projected augmented waves basis set [30] and periodic boundary conditions. The MoO_2/Mo(110) system, which has been previously simulated elsewhere [29], consists of the O-Mo-O trilayer atop three layers of Mo(110) and a 15 Å vacuum gap. This model was then used as a "substrate" to simulate the Fe nanoclusters on the MoO_2/Mo(110) surface. The electron exchange and correlation were simulated by local density approximation pseudopotentials with a Ceperley-Alder exchange functional [31]. The Γ-point was used to sample the Brilliouin zone. The energy cut-off used for all calculations was 300 eV. For the density of states, a smearing of 0.2 eV was applied using the Methfessel-Paxton method. The global break condition for the electronic self-consistent loops was set to a total energy change of less than 10^{-6} eV. The Mo layer furthest from the surface was constrained to simulate bulk Mo and the unit cell was allowed to relax by minimising the total forces on each ion to less than 0.01 eV/Å.

Nanoclusters which contain 1 to 6 Fe atoms were considered in order to fit an experimentally observed cluster size with a width of 6 Å. All Fe/MoO_2/Mo(110) systems were relaxed prior to any further calculations. Simulations of 1, 2, 3, 4 and 6 atoms have shown that after the atom positions were relaxed, some of the Fe atoms ended up mixed into the MoO_2 layer. This suggests bonding occurs between Fe and MoO_2. Such diffusion and subsequent bonding can be ruled out by the previously reported X-ray absorption spectroscopy measurements [32]; spectra of the MoO_2/Mo(110) surface after deposition of 0.7 ML of Fe demonstrated metallic character, indicating Fe nucleates atop the oxygen rows. The Fe cluster with 5 atoms was found to be the most resistant to diffusion into the substrate, had the lowest energy, and exhibited a width of 6 Å, which is in good agreement with the experimental data. Four different starting configurations (geometrical positions) for the Fe nanocluster consisting of 5 atoms have been examined. The most favourable relaxed model of the Fe nanocluster on the MoO_2/Mo(110) surface is shown in figures 3(a) and (b). The other three orientations either did not resemble the experimentally observed geometrical structure or had a higher energy than that of the structure shown in figure 3(a) and (b). In order to further compare the DFT results with our STM images, the partial charge density of the Fe on the MoO_2/Mo(110) surface has been simulated in the range between the Fermi energy (E_F) and 1 V. The calculated image is compared with

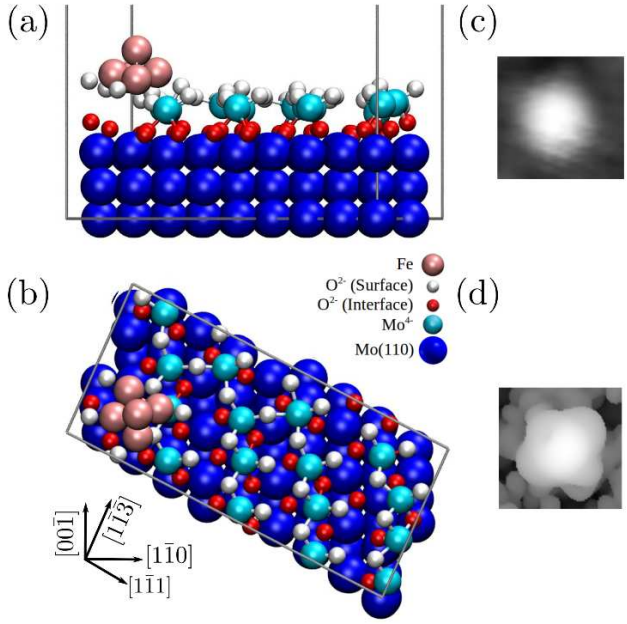

Figure 3. Side (a) and top (b) views of the calculated relaxed Fe/MoO_2/Mo(110) structure. The grey rectangular grid represents the overlayer unit cell. (c) Occupied state STM image of the Fe nanocluster (1.4 nm × 1.4 nm, $V_b = 1$ V), compared to (d) the simulated partial charge density (from E_F to 1 V).

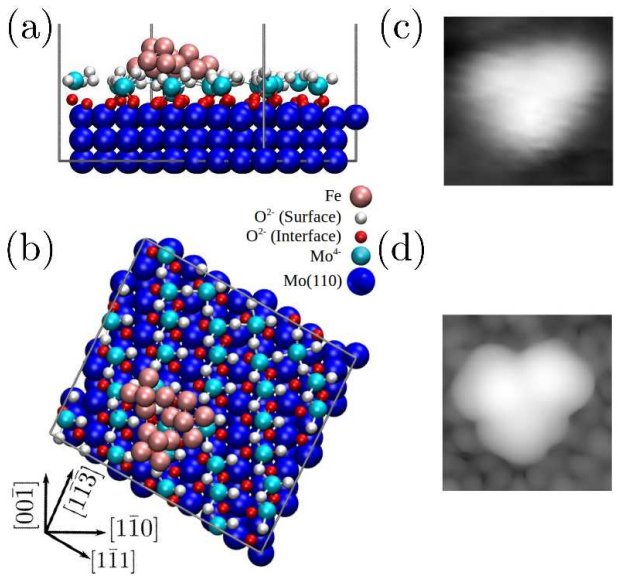

Figure 4. Side (a) and top (b) views of the calculated relaxed three nanoclusters each composed of 5 Fe atoms on the MoO_2/Mo(110) structure. The grey rectangular grid represents the overlayer unit cell. (c) Occupied state STM image of the Fe nanostructure (1.4 nm × 1.4 nm, $V_b = 1$ V) compared to (d) the simulated partial charge density (from E_F to 1 V).

an STM image obtained at a bias voltage of 1 V in figures 3(c) and (d). Its size and overall shape show very good agreement. However, the simulated image exhibits more features than the measured STM image. The reason for this could be the neglect of tip-sample convolution within partial charge density simulations.

To investigate whether the larger Fe structures are comprised of multiples of these 5-atom clusters, a triangular nanostructure (see figure 1(a) inset) consisting of three 5-atom clusters was simulated. The MoO_2/Mo(110) slab size was doubled in the [1$\bar{1}\bar{3}$] direction to accommodate the triangular Fe nanocomposite. Three of the 5-atom nanoclusters were arranged in a triangle and the system was allowed to relax. As can be seen in the relaxed model in figure 4(a) and (b), the 5-atom clusters are stable even when in close proximity to one another. Each cluster is clearly separated from its neighbours, which suggests that for this system, 5 atoms is a "magic number" where the cohesion of the cluster is maximised. In order to further compare the DFT results with the STM images, the partial charge density of the triangular Fe structure on the MoO_2/Mo(110) surface has been simulated in the range between the Fermi energy (E_F) and 1 V. Figures 4(c) and (d) shows the comparison of the calculated image with an STM image obtained at a bias voltage of 1 V. The two images are in very good agreement, with the size, shape and internal structure reproduced, suggesting that the observed triangular Fe nanostructures consist of three smaller 5-atom clusters. Furthermore, these calculations indicate that all the Fe nanostructures on the MoO_2/Mo(110) surface at low coverage consist of several 5-atom clusters.

The models presented in figures 3 and 4 helps to understand the preferred formation of the triangular shaped composites consisting of three 5-atom Fe nanoclusters at low surface coverage. The four-atom bottom layer of each Fe nanocluster resembles the Fe(001) surface and is oriented on the substrate in such a way that its diagonals are along [00$\bar{1}$] and [1$\bar{1}$0] directions of the Mo(110) surface. Each of these four Fe atoms occupies a position between three oxygen atoms that form the top layer of the MoO_2 surface. The same applies when three such 5-atom Fe nanoclusters join in a triangular composite. Due to the limited space between the rows of top-layer oxygen atoms which run along the [00$\bar{1}$] direction on the MoO_2/Mo(110) surface, the Fe atoms forming a bottom layer in a three-cluster composite are pulled together in the middle (surface stress) and pushed away from the centre to the periphery of the composite (surface strain). This minimizes a nucleation probability of additional 5-atom Fe nanoclusters around the three-cluster composite at low coverage.

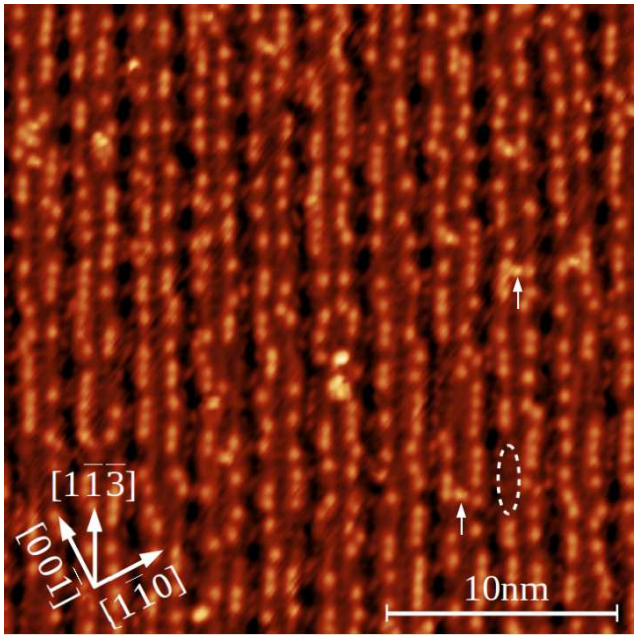

Figure 5. An experimental STM image of the MoO_{2+x}/Mo(110) surface (25 nm × 25 nm, $V_b = 1.5$ V, $I_t = 1$ nA). The extra oxygen appears as bright protrusions in the image and clearly forms a double row structure on top of the MoO_2 layer. The average distances between two adjacent oxygen adatoms along and perpendicular to the nanorow direction are approximately 1 nm and 1.3 nm, respectively, and are dictated by the strained MoO_2(010) layer. The dashed oval and the arrows illustrate a patch with no oxygen adatoms and misplaced oxygen adatoms, respectively

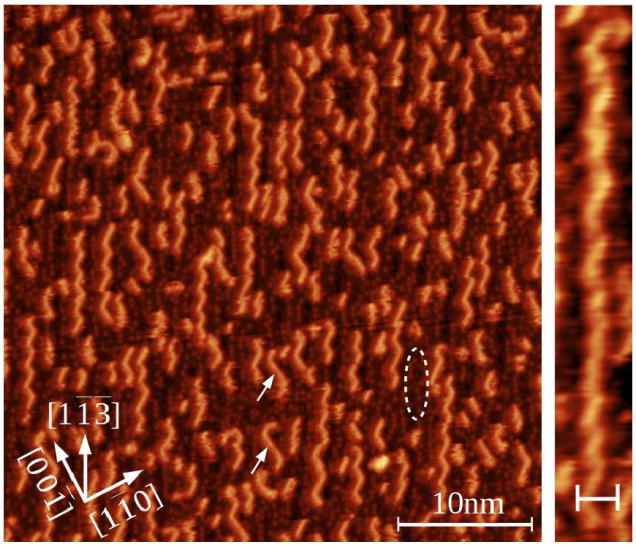

Figure 6. STM images of 0.5 ML of Fe on MoO_{2+x}/Mo(110) (40 nm × 40 nm, V_b = - 0.5 V, I_t = 1.10 nA). Deposition of Fe on the MoO_{2+x}/Mo(110) surface leads to the formation of elongated nanolines (left panel), which have a zigzag shape and are up to 24 nm in length (right panel). The scale bar in the right panel indicates 2 nm. The dashed oval illustrates a gap between the zigzag nanolines due to the absence of oxygen adatoms. The arrows illustrate examples of zigzags nanolines crossing from one side of the Mo oxide nanorow to the other due to the presence of misplaced oxygen adatoms.

3.2. Growth of Fe on the MoO_{2+x} surface

Altering the preparation of the MoO_2/Mo(110) surface slightly (see Section 2) leads to the existence of oxygen adatoms atop the MoO_2 structure. An STM image of this oxygen-rich surface, which is denoted as MoO_{2+x}/Mo(110) [29], is presented in figure 5. The oxygen adatoms are adsorbed on top of the Mo oxide nanorows [29], forming a perfectly aligned double row structure. The average distances between two adjacent oxygen adatoms along and perpendicular to the nanorow direction are approximately 1 nm and 1.3 nm, respectively, and are dictated by the strained MoO_2(010) layer [28, 29].

In contrast to the small clusters discussed in the previous section, the deposition of 0.5 ML of Fe on the MoO_{2+x}/Mo(110) surface leads to the formation of elongated nanolines, which have a zigzag shape and are up to 24 nm in length (figure 6). The direction of the "zig" and "zag" sections of the nanolines corresponds to the lattice directions of the topmost oxygen layer of the MoO_2 structure [28]. Similarly to the oxygen adatoms, the nanolines tend to follow the [1$\bar{1}\bar{3}$] direction. A comparison between the STM images presented in figures 5 and 6 suggests that the zigzag shaped nanolines form around the oxygen adatoms on the MoO_{2+x} surface. Each Mo oxide nanorow is 2.5 nm wide and accommodates two parallel rows of oxygen adatoms (figure 5) and zigzag nanolines (figure 6) before and after Fe deposition, respectively.

The presence of oxygen adatoms is clearly a prerequisite for the formation of the zigzag nanolines, as the deposition of Fe on the MoO_2 leads to the existence of small nanoclusters (figure 1). Furthermore, after deposition of Fe onto oxygen-rich MoO_{2+x}/Mo(110) no oxygen adatoms have been observed on the surface as single separate units. Therefore, it is suggested that Fe interacts with the oxygen adatoms to form partially oxidized Fe nanolines on the MoO_{2+x}/Mo(110) surface. The formation of the zigzag shape can be understood by considering that the position of Fe atoms on the surface is defined by oxygen atoms forming the topmost MoO_2 layer. The Fe atoms connected to the oxygen atoms of the topmost layer form the base of the zigzag nanoline. When there are no oxygen adatoms on the surface it results in a formation of Fe nanocluster composites (figure 1) most of which have a triangular shape (figure 1(b)). These nanoclusters are the starting point of a zigzag structure which only require a bridging element between them to form a segment of the zigzag nanoline. The oxygen adatoms on the MoO_{2+x}/Mo(110) surface act as such bridging elements. They are stable on the surface being bonded to the Mo atoms which are slightly lifted from the MoO_2 layer as a result of this extra bond [29]. However, these adatoms can be easily removed from the surface by scanning (or pulsing) at positive sample biases greater than 1.5 V due to inelastic electron tunnelling [29]. That makes the oxygen adatoms perfect candidates as bridging elements for the observed zigzag nanolines because they are able to migrate when the electrons necessary for bonding are provided. The oxygen adatoms form rows runnning in the [1$\bar{1}\bar{3}$] direction (figure 5) which are rotated by approximately 30° clockwise and anticlockwise to the two lattice directions of the underlying oxygen layer. This results in the formation of nanolines running along the [1$\bar{1}\bar{3}$] direction of the substrate with the zigzag line segments following the lattice directions of the underlying oxygen layer. The length and the shape of the zigzag nanolines strongly depend on the coverage of oxygen adatoms. Patches with no oxygen adatoms on the oxygen-rich MoO_{2+x}/Mo(110) surface (dashed oval in figure 5) result in gaps between zigzag nanolines along the [1$\bar{1}\bar{3}$] direction of the substrate (dashed oval in figure 6). Defects or misplaced oxygen adatoms located in the middle of the Mo oxide nanorows (arrows in figure 5) result in zigzag nanolines crossing from one side of the Mo oxide nanorow to the other (arrows in figure 6). Additional X-ray absorption and photoemission measurements and DFT calculations will help shed light on the stoichiometry and properties of these partially oxidized Fe nanolines.

4. Conclusion

The results obtained demonstrate that the Fe nanostructures of varying size and shape can be synthesized on molybdenum oxide surfaces. At low coverage, Fe self-assembles into small well-separated nanoclusters on the MoO_2/Mo(110) surface. DFT simulations show that they consist of 5 Fe atoms. These 5-atom clusters can agglomerate to form structures of varying size and shape which consist of 2 to 6 clusters. At low surface coverage there is a clear preference for triangular composite structures that consist of 3 Fe nanoclusters due to the MoO_2 lattice. Linear Fe nanocluster arrays that follow the Mo oxide rows are formed on the MoO_2/Mo(110) surface at room temperature if the Fe coverage exceeds 0.6 ML. In turn, the deposition of Fe on the oxygen-rich MoO_{2+x}/Mo(110) surface leads to the formation of continuous, zigzag-shaped nanolines with lengths of up to 24 nm. It is suggested that these nanolines are formed of partially oxidized Fe, and oxygen adatoms on the surface control the length and spatial distribution of zigzag nanostructures. Altering the oxygen content of the molybdenum oxide surface leads to the existence of nanostrucutres with different sizes, structures and chemical compositions. Therefore, this molybdenum oxide surface provides an excellent template for the growth and investigation of different nanostructures.

Acknowledgments

This work was supported by Science Foundation Ireland through the Principal Investigator grants (SFI P.I. 09/IN.1/I2635 and SFI P.I. 12/IA/1264). The authors thank Trinity College High Performance Cluster, funded by the Higher Education Authority under the Program for Research in Third Level Institutes, and Dell Computers (Ireland) Ltd. for computing resources.

References

[1] Gao M R, Xu Y F, Jiang J and Yu S H 2013 *Chem. Soc. Rev.* **42** 2986
[2] Yu R, Lin Q, Leung S F and Fan Z 2012 *Nano Energy* **1** 57–72
[3] Zhu C, Yang G, Li H, Du D and Lin Y 2015 *Anal. Chem.* **87** 230–249
[4] Wang Z 2007 *Appl. Phys. A* **88** 7–15
[5] Qiao Z A, Wu Z and Dai S 2013 *Chem. Sus. Chem.* **6** 1821–1833
[6] Zeng J, Zhang Q, Chen J and Xia Y 2010 *Nano Lett.* **10** 30–35
[7] Cargnello M, Doan-Nguyen V V T, Gordon T R, Diaz R E, Stach E A, Gorte R J, Fornasiero P and Murray C B 2013 *Science* **341** 771–773
[8] Topsøe H 2007 *Appl. Catal., A* **322** 3 – 8
[9] Duan J, Chen S, Dai S and Qiao S Z 2013 *Adv. Funct. Mater.* **24** 2072–2078
[10] An K and Somorjai G A 2012 *Chem. Cat. Chem.* **4** 1512–1524
[11] Bell A T 2003 *Science* **299** 1688–1691
[12] Besenbacher F, Lauritsen J V and Wendt S 2007 *Nano Today* **2** 30–39
[13] Valden M, Lai X and Goodman D W 1998 *Science* **281** 1647–1650
[14] Yeung K L and Yao N 2004 *J. Nanosci. Nanotechnol.* **4** 647–690
[15] Kolb M J, Farber R G, Derouin J, Badan C, Calle-Vallejo F, Juurlink L B F, Killelea D R and Koper M T M 2016 *Phys. Rev. Lett.* **116** 136101
[16] Inukai J, Tryk D A, Abe T, Wakisaka M, Uchida H and Watanabe M 2013 *J. Amer. Chem. Soc.* **135** 1476–1490
[17] Minato T, Susaki T, Shiraki S, Kato H S, Kawai M and Aika K 2004 *Surf. Sci.* **566-568** 1012–1017
[18] Wallace W, Min B and Goodman D 2005 *J. Mol. Catal. A: Chem.* **228** 3–10
[19] Jennings J 1991 *Catalytic Ammonia Synthesis: Fundamentals and Practice* Fundamental and Applied Catalysis (Springer)
[20] Adkins H and Peterson W R 1931 *J. Am. Chem. Soc.* **53** 1512–1520
[21] Campbell C T 2006 *Phys. Rev. Lett.* **96** 066106
[22] Gustafson J, Mikkelsen A, Borg M, Lundgren E, Köhler L, Kresse G, Schmid M, Varga P, Yuhara J, Torrelles X, Quirós C and Andersen J N 2004 *Phys. Rev. Lett.* **92** 126102
[23] Gustafson J, Mikkelsen A, Borg M, Andersen J N, Lundgren E, Klein C, Hofer W, Schmid M, Varga P, Kohler L, Kresse G, Kasper N, Stierle A and Dosch H 2005 *Phys. Rev. B* **71** 115442
[24] Todorova M, Li W X, Ganduglia-Pirovano M V, Stampfl C, Reuter K and Scheffler M 2002 *Phys. Rev. Lett.* **89** 096103
[25] Diebold U 2003 *Surf. Sci. Rep.* **48** 53 – 229
[26] Chaika A N, Nazin S S, Semenov V N, Bozhko S I, Lübben O, Krasnikov S A, Radican K and Shvets I V 2010 *Europhys. Lett.* **92** 46003
[27] Chaika A N, Orlova N N, Semenov V N, Postnova E Y, Krasnikov S A, Lazarev M G, Chekmazov S V, Aristov V Y, Glebovsky V G, Bozhko S I and et al 2014 *Sci. Rep.* **4** 3742
[28] Radican K, Berdunov N, Manai G and Shvets I V 2007 *Phys. Rev. B* **75**(15) 155434
[29] Krasnikov S, Lübben O, Murphy B, Bozhko S, Chaika A, Sergeeva N, Bulfin B and Shvets I 2013 *Nano Res.* **6** 929–937
[30] Kresse, G and Furthmüller, J 1996 *Phys. Rev. B* **54** 11169–11186
[31] Ceperley D M and Alder B J 1980 *Phys. Rev. Lett.* **45** 566–569
[32] Lübben O, Krasnikov S A, Preobrajenski A B, Murphy B E, Bozhko S I, Arora S K and Shvets I V 2012 *J. Appl. Phys.* **111** 07B515